Stereoselective Formation of Facial Tris-cyclometalated Pt(IV) Complexes. Dual Phosphorescence from Heteroleptic Derivatives

Juan Carlos López-López,[a] Delia Bautista,[b] and Pablo González-Herrero*[a]

Abstract: A stereoselective synthetic route to homo- and heteroleptic facial tris-cyclometalated Pt(IV) complexes is reported, involving the oxidative addition of 2-(2-pyridyl)- or 2-(1-isoquinolinyl)benzenediazonium salts to *cis*-[Pt(C^N)$_2$] precursors, with C^N = cyclometalated 2-(*p*-tolyl)pyridine (tpy), 2-phenylquinoline (pq), 2-(2-thienyl)pyridine or 1-phenylsioquinoline (piq), to produce labile diazenide intermediates that undergo photochemical or thermal elimination of N_2. The method allows the preparation of derivatives bearing cyclometalated ligands of low π-π^* transition energies. The new complexes exhibit phosphorescence in fluid solution at room temperature arising from triplet ligand-centred (^{3}LC) excited states, which, in the cases of the heteroleptic derivatives, involve the ligand with the lowest π-π^* gap. The heteroleptic piq derivatives exhibit fluorescence and dual phosphorescence from different ligand-centred excited states in rigid media, demonstrating the potential of cyclometalated Pt(IV) complexes as multi-emissive materials.

Introduction

Transition metal tris chelates bearing heterocyclic aromatic ligands have played a fundamental role in the field of photophysics and photochemistry of coordination compounds because of the high tunability and wide applicability of their excited-state properties. Complexes of the d^6 ions Ru(II)[1] and Ir(III)[2] with 2,2'-bipyridyls (N^N) and/or cyclometalated 2-arylpyridines (C^N) stand out as the most studied tris chelates due to their use as photosensitizers in diverse light-based processes,[3–5] photocatalysts for hydrogen production[6,7] and organic synthesis[8,9] or phosphorescent dopants for electroluminescent devices.[10–12] Recent work from our laboratory has shown that facial isomers of tris-cyclometalated Pt(IV) complexes with 2-arylpyridines, *fac*-[Pt(C^N)$_3$]$^+$, may exhibit efficient and long-lived luminescence from essentially ligand-centred triplet excited states (^{3}LC) with very little metal-to-ligand charge-transfer (MLCT) character,[13–15] making them promising candidates for applications that benefit from prolonged excited-state lifetimes, such as chemosensing, photosensitizing or photocatalysis. The reported synthetic procedure involves the abstraction of the chloride ligands from C_2-symmetrical isomers of complexes [PtCl$_2$(C^N)$_2$] with 2 equiv. of AgOTf in the presence of a third 2-arylpyridine ligand at 90-140 °C in noncoordinating solvents, affording exclusively the meridional isomers, *mer*-[Pt(C^N)$_3$]$^+$, which must then be converted to the *fac* isomers via photoisomerization using UV light. However, this method has two key disadvantages that have hindered further developments: the photoisomerization step often results in low yields due to partial decomposition and C^N ligands of low π-π^* transition energies cannot be employed because they lead to reduction to Pt(II) under the reaction conditions, greatly hampering excited-state tunability. Alternative routes to *fac*-[Pt(C^N)$_3$]$^+$ complexes would thus be highly desirable. In addition, we have sought the synthesis of heteroleptic complexes to examine the effects of the presence of different ligand combinations on their luminescence. Mixed-ligand tris chelates have been of particular interest with the Ir(III) ion as a strategy to fine-tune their photophysical properties[16] and the design of multifunctional phosphorescent molecules[17] or possible dual emitters for the fabrication of white organic light-emitting devices (WOLEDs).[18]

In this work, we examine the suitability of *cis*-[Pt(C^N)$_2$] complexes[19] as precursors and the use of 2-(2-pyridyl)arenediazonium salts to introduce the third cyclometalated ligand. The ability of *cis*-[Pt(C^N)$_2$] complexes to undergo thermal or photochemical oxidations under mild conditions is well known,[20,21] although it has never been exploited for the synthesis of Pt(IV) tris chelates. On the other hand, arenediazoniums are electrophilic reagents that have proved useful for the synthesis of aryl complexes.[22–29] Of particular significance to the present study are the reported oxidative additions of 2-(2-pyridyl)benzenediazonium to Au(I) species under visible-light photocatalytic conditions to give cyclometalated Au(III) complexes, in which the initial one-electron reduction of the diazonium is effected by the photocatalyst to give an aryl radical with loss of N_2.[23] Oxidative additions of arenediazoniums to Au(I) complexes have also been reported to proceed under visible-light irradiation in the absence of a photocatalyst with formation of Au(III) aryl derivatives.[24,25] In these cases, Au(III) species bearing an aryldiazenide ligand (ArN_2^-) have been proposed as the key intermediates that undergo the photoelimination of N_2, but they were not isolated. Arenediazoniums are also known to oxidatively add to complexes of several metal ions, including Ru(II),[30] Ir(I)[31] or Pd(II),[32] to give aryldiazenide complexes. As far as we are aware, there is only one report describing the oxidative addition of an arenediazonium to a Pt(II) species, which gives a labile aryldiazenide Pt(IV) complex that easily undergoes N_2 elimination.[33]

[a] J. C. López-López, Dr. P. González-Herrero
Departamento de Química Inorgánica, Facultad de Química
Universidad de Murcia
Campus de Espinardo, 19, 30100 Murcia (Spain)
E-mail: pgh@um.es

[b] Dr. D. Bautista
ACTI, Universidad de Murcia
Campus de Espinardo, 21, 30100 Murcia (Spain)

Supporting information for this article is given via a link at the end of the document.

Results and Discussion

Synthesis and characterization

We initially tested the reaction of *cis*-[Pt(tpy)$_2$] (**1a**; see Scheme 1 for ligand name abbreviations) with 5-methyl-2-(2-pyridyl)benzenediazonium tetrafluoroborate (tpyN$_2$BF$_4$) in 1:1 molar ratio in MeCN at room temperature under irradiation with blue LEDs (λ_{max} = 454 nm) for 24 h. The obtained crude material was a mixture of mainly *fac*- and *mer*-[Pt(tpy)$_3$]BF$_4$ (*fac/mer*-**3aa**) in 1:2 molar ratio. The cations *fac/mer*-[Pt(tpy)$_3$]$^+$ have been already reported[13] and were identified by their ^{1}H NMR data, which show one (*fac*) or three (*mer*) distinctive aromatic resonances in the range 5.94–6.54 ppm arising from the protons ortho to the metalated carbon atoms, that are considerably shielded by the diamagnetic current of orthogonal aromatic rings. Further attempts were carried out under the same conditions by reacting *cis*-[Pt(thpy)$_2$] (**1c**) with tpyN$_2$BF$_4$ or 2-(1-isoquinolinyl)benzenediazonium tetrafluoroborate (piqN$_2$BF$_4$), which gave mixtures containing mainly *fac*-[Pt(thpy)$_2$(C'^N')]BF$_4$ [C'^N' = tpy (*fac*-**3ca**), piq (*fac*-**3cd**)] and another complex, tentatively assigned as the *mer* isomer, in 7.3:1 or 4:1 ratios, respectively, whereas the reaction of *cis*-[Pt(piq)$_2$] (**1d**) with (piqN$_2$BF$_4$) gave *fac*-[Pt(piq)$_3$]BF$_4$ (*fac*-**3dd**) as the only tris-cyclometalated Pt(IV) complex, which was isolated in 42% yield.

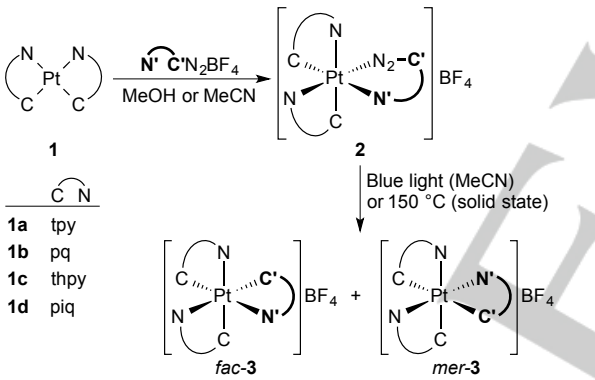

Photochemical method:

C^N	C'^N'	Product(s)	*fac:mer* ratio
tpy	tpy	*fac/mer*-**3aa**	1:2
thpy	tpy	*fac/mer*-**3ca**	7.3:1
thpy	piq	*fac/mer*-**3cd**	4:1
piq	piq	*fac*-**3dd**	–

Thermal method:

C^N	C'^N'	Product	Yield (%) MeOH	MeCN
tpy	tpy	*fac*-**3aa**	60	33
tpy	piq	*fac*-**3ad**	62	43
pq	tpy	*fac*-**3ba**	38	47
pq	piq	*fac*-**3bd**	43	53
thpy	tpy	*fac*-**3ca**	42	39
thpy	piq	*fac*-**3cd**	37	37
piq	tpy	*fac*-**3da**	41	33
piq	piq	*fac*-**3dd**	69	57

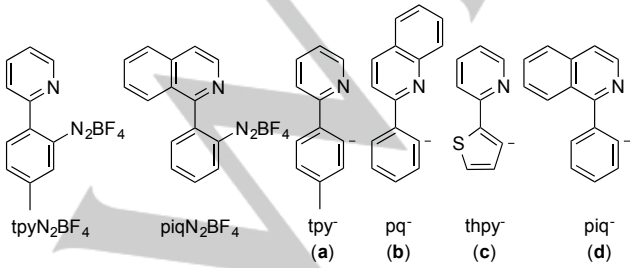

Scheme 1. Photochemical and thermal syntheses of tris-cyclometalated Pt(IV) complexes via diazenide intermediates.

The described photochemical method was thus not generally suitable for the direct synthesis of *fac*-[Pt(C^N)$_3$]$^+$ complexes, because the *mer* isomer can also form and, in our experience, it cannot be separated by chromatography. To investigate which conditions could favour the formation of the *fac* isomer, we attempted the isolation of possible intermediates by carrying out the reactions in the dark, but the obtained products could not be conveniently purified because of their instability in solution. The use of MeOH instead of MeCN as solvent resulted in purer products, but only in the case of the reaction of **1c** with tpyN$_2$BF$_4$ could an analytically pure sample be obtained, whose elemental analysis was consistent with the formulation [Pt(thpy)$_2$(N$_2$tpy)]BF$_4$ (**2ca**). Its ^{1}H NMR spectrum showed the presence of two inequivalent cyclometalated thpy ligands and a non-metalated *p*-tolyl group, consistent with a Pt(IV) complex bearing a diazenide ligand resulting from the oxidative addition of tpyN$_2^+$. Importantly, these data also demonstrated the selective formation of a single geometrical isomer. The ESI(+) mass spectrum corroborated the presence of the [Pt(thpy)$_2$(N$_2$tpy)]$^+$ cation at m/z 711.0928, and showed an additional peak at m/z 683.0869, corresponding to [Pt(thpy)$_2$(tpy)]$^+$, resulting from the loss of N$_2$. Complex **2ca** was confirmed as the intermediate in the photochemical synthesis of *fac*-**3ca** by irradiating a solution in CD$_3$CN with blue LEDs, which led to the tris-cyclometalated complex.

Since crystallization of intermediates **2** failed as BF$_4^-$ salts, we attempted the use of the BPh$_4^-$ anion. The isolation of [Pt(tpy)$_2$(N$_2$tpy)]BPh$_4$ (**2aa-BPh$_4$**) was possible from the reaction with **1a** with tpyN$_2$BPh$_4$ in MeOH. Its ^{1}H NMR spectrum showed resonances arising from three inequivalent *p*-tolyl groups, consistent with a single geometrical isomer. A single-crystal X-ray diffraction analysis revealed a Pt(IV) complex cation bearing two tpy ligands in an unsymmetrical arrangement and a 5-methyl-2-(2-pyridyl)benzenediazenide ligand coordinated through the azo and pyridine groups, forming a seven-membered chelate ring (Figure 1). The three pyridine groups are in a *fac* configuration, meaning that the selectively formed isomer should be ideally suited to produce the *fac* tris-cyclometalated Pt(IV) complex after N$_2$ elimination.

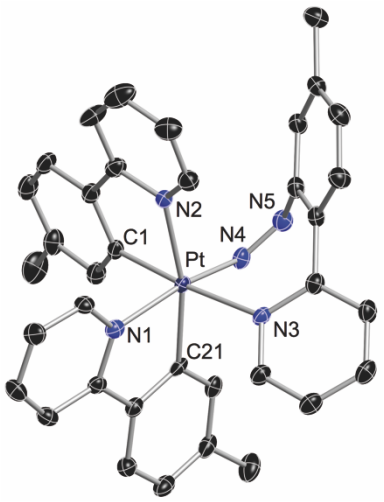

Figure 1. Structure of the cation of **2aa-BPh$_4$** in the crystal. Hydrogen atoms are omitted. Selected bond distances (Å) and angles (°): Pt-C1 2.016(2), Pt-C21 2.018(2), Pt-N4 2.052(2), Pt-N2 2.152(2), Pt-N1 2.160(2), Pt-N3 2.182(2), N4-N5 1.219(3), C1-Pt-N2 80.02(10), C21-Pt-N1 80.22(9), N4-Pt-N3 89.29(8), N5-N4-Pt 123.94(19).

In view of the structure of **2aa-BPh$_4$**, we hypothesized that the formation of a proportion of *mer* isomer upon irradiation in solution could result from the decoordination of the pyridine group of the diazenide ligand before or during the photoelimination of N_2, possibly producing uncoordinated tpy· radicals, that could combine with the bis-cyclometalated metal fragment in two different orientations. We thus considered to induce the N_2 elimination thermally in the solid state. A thermogravimetric analysis of **2ca** showed a 3.5% weight loss, corresponding to an N_2 molecule, peaking at 151.7 °C (Figure S17, Supporting Information). Gratifyingly, the heating of a solid sample of **2ca** at 150 °C for 3 h selectively afforded *fac*-**3ca**, which could be isolated in moderate yield after purification through column chromatography. A general protocol was then employed for the direct synthesis of a series of homo- and heteroleptic *fac* tris-cyclometalated Pt(IV) complexes (Scheme 1), involving the reaction of complexes **1** with the diazonium salt in MeOH or MeCN, precipitation of the diazenide intermediate and thermal elimination of N_2 in the solid state. No traces of the *mer* isomers were detected in the crude reaction products. The use of MeOH as solvent for the generation of the diazenide led to significantly increased yields in particular cases (*fac*-**3aa** and **3ad**), probably because of the higher stability of the intermediate in this solvent. The *fac* configuration of the heteroleptic complexes was confirmed by their ^{1}H NMR data, which show three shielded resonances with Pt satellites arising from the protons ortho to the metalated carbon atoms, two of them at very similar chemical shifts. The crystal structure of the homoleptic piq complex *fac*-**3dd** was solved as the BPh_4^- salt (Figure 1). It is the first reported structure of a tris-cyclometalated Pt(IV) complex with a *fac* configuration. The rather short Pt–C bond distances (range 1.993–2.011 Å) are comparable to other Pt–C distances trans to N in cyclometalated Pt(IV) complexes.[13,34]

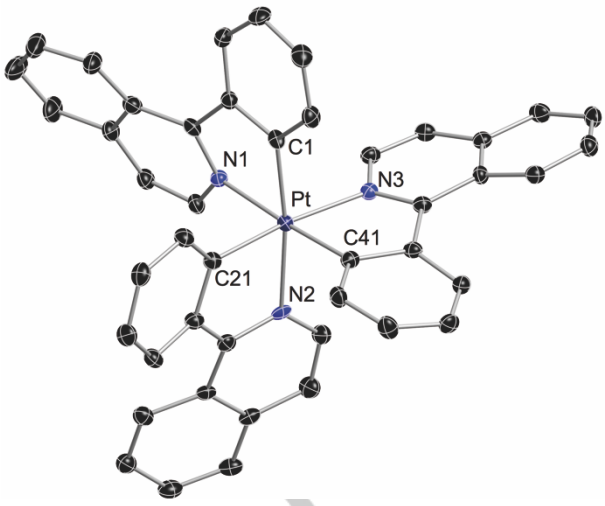

Figure 2. Structure of the cation of *fac*-**3dd-BPh$_4$** in the crystal. Hydrogen atoms are omitted. Selected bond distances (Å) and angles (°): Pt-C1 1.993(4), Pt-C41 2.007(4), Pt-C21 2.011(4), Pt-N3 2.128(3), Pt-N1 2.130(3), Pt-N2 2.146(4), C1-Pt-N1 80.04(15), C21-Pt-N2 81.14(15), C41-Pt-N3 80.52(15).

Photophysical study

The electronic absorption spectra of complexes *fac*-**3** in CH_2Cl_2 solution at 298 K show structured bands (Figure 2, Table S2, Supporting Information) in the range 300-400 nm attributable to singlet ligand-centred (^{1}LC or $^1\pi$-π^*) transitions.[13,14,34–36] The characteristic maxima from the individual ligands can be identified by comparing the different spectra, appearing at *ca.* 363 and 378 nm (piq), 361 nm (thpy), 351 and 365 nm (pq) or 314, 326 and 340 nm (tpy). An additional low-energy feature is observed as a very weak shoulder or tail, assignable to ligand-to-ligand charge-transfer (LLCT) transitions on the basis of TDDFT calculations (see below).

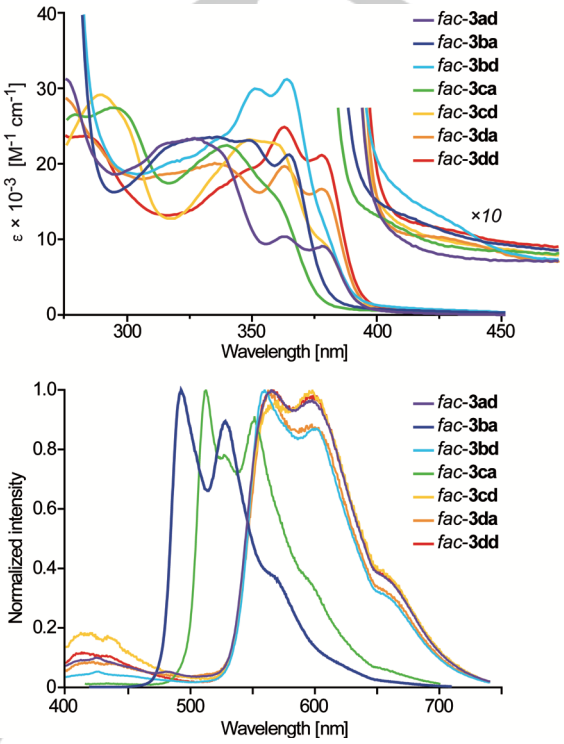

Figure 3. Absorption (top) and emission (bottom) spectra of complexes *fac*-**3** in CH_2Cl_2 solution at 298 K.

Table 1 summarizes the luminescence data of the new complexes in deaerated CH_2Cl_2 solutions and poly(methyl methacrylate) (PMMA) matrices (2 wt%) at 298 K and in butyronitrile (PrCN) glasses at 77 K. The complete set of excitation and emission spectra is included in the Supporting Information. All complexes give rise to a vibrationally structured emission band in CH_2Cl_2 solution as the major feature (Figure 2), characterized by large Stokes shifts and microsecond lifetimes, consistent with ^{3}LC emitting states. In accord with Kasha's rule,[37] the chromophoric ligand in the heteroleptic complexes is the one with the lowest π-π^* transition energy, i.e., pq in *fac*-**3ba**, thpy in *fac*-**3ca** and piq in *fac*-**3ad**, **3bd**, **3cd** and **3da**, as deduced by comparison with other cyclometalated Pt(IV) emitters bearing these ligands.[14,35,38,39] The excitation spectra faithfully reproduce the absorption profiles in all cases (Figure S18, Supporting Information). An additional band is observed at a higher energy (400-450 nm) for all the piq derivatives, which can be ascribed to fluorescence from a ^{1}LC(piq) state on the basis of its small Stokes shift and very short lifetime (<0.2 ns), implying that intersystem crossing to and radiative decay from the piq-centred triplet state are less efficient as compared with the pq- or thpy-centred triplet

states, which results in fluorescence becoming competitive.[14,15] This behaviour can be attributed to the diminished spin-orbit coupling induced by the metal because of its proportionally lower orbital contribution to the piq-centred excited state. The pq-centred emitter *fac*-**3ba** exhibits the highest emission quantum yield of the present series in fluid solution (0.20). The thpy- and piq-centred emitters show appreciably lower efficiencies, suggesting an important nonradiative deactivation as a consequence of the energy gap law.[40]

Table 1. Emission data for complexes *fac*-**3**.

Complex	Medium (T [K])	λ_{em} [nm][a]	τ [μs][b]	Φ[c]
fac-**3ad**	CH_2Cl_2 (298)	564	11	0.029
	PMMA (298)	487, 558	40 (38), 93 (62)	0.046
	PrCN (77)	481, 554	79 (72), 205 (28)	
fac-**3ba**	CH_2Cl_2 (298)	493	24	0.20
	PMMA (298)	491	266	0.46
	PrCN (77)	488	333	
fac-**3bd**	CH_2Cl_2 (298)	569	9.4	0.014
	PMMA (298)	487, 553	30 (15), 107 (85)	0.054
	PrCN (77)	491, 545	96 (47), 168 (53)	
fac-**3ca**	CH_2Cl_2 (298)	513	28	0.065
	PMMA (298)	512	236	0.23
	PrCN (77)	509	415	
fac-**3cd**	CH_2Cl_2 (298)	564	17	0.027
	PMMA (298)	561	37 (41), 88 (59)	0.043
	PrCN (77)	552	37 (32), 104 (68)	
fac-**3da**	CH_2Cl_2 (298)	568	17	0.021
	PMMA (298)	561	50	0.042
	PrCN (77)	482, 558	70 (78), 259 (22)	
fac-**3dd**	CH_2Cl_2 (298)	563	15	0.036
	PMMA (298)	563	50	0.039
	PrCN (77)	557	77	

[a] Highest-energy peak of the phosphorescence band(s). [b] Relative amplitudes (%) are given in parentheses for biexponential decays. [c] Absolute quantum yield.

The emission profiles in PMMA are very similar to those in CH_2Cl_2 solution except for derivatives *fac*-**3ad**, **3bd** and **3da**, which give rise to additional peaks between the piq-centred fluorescence and phosphorescence bands. To exclude the presence of trace impurities as their origin, these heteroleptic derivatives were doubly purified by chromatography. When registered in PrCN at 77 K, the spectra show the characteristic sharply structured pq-, thpy- or piq-centred phosphorescence bands as the main feature (Figure S20, Supporting Information). Also in this medium, complexes *fac*-**3ad**, **3bd** and **3da** show additional peaks when excited at the lowest-energy absorption maximum, which become particularly intense for *fac*-**3ad** and **3da** (Figure 3), allowing a more detailed study in these cases. This additional emission has the same shape and energy for both derivatives, although it is more intense for *fac*-**3ad**, bearing two tpy ligands, than for *fac*-**3da**, bearing only one. Excitation at different wavelengths revealed variations in the relative intensity of this emission. Notably, excitation at the ^{1}LC(tpy) absorption wavelength (343 nm) allowed the observation of its 0–0 peak at 452 nm, which coincides with that of *fac*-$[Pt(tpy)_3]^+$[13] and thus can be ascribed to a ^{3}LC state involving the tpy ligand. Similarly, the highest-energy additional peak observed for *fac*-**3bd** occurs at 491 nm, matching the pq-centred emission of *fac*-**3ba**. The excitation profiles monitored at the tpy-centred emission at 77 K for *fac*-**3ad** and **3da** are almost identical to those obtained at the piq-centred fluorescence and phosphorescence bands (Figures S21 and S22, Supporting Information), which supports that the different emissions originate from a single species. However, the relative intensity of the lowest-energy excitation band, which may correspond to a ^{1}LLCT absorption, is higher for the tpy-centred emission, suggesting that low-lying ^{1}LLCT states may provide a route for the population of the emissive ^{3}LC(tpy) state. Lifetimes registered at the piq-centred phosphorescent emission resulted in all cases in biexponential decays in the microsecond range, consistent with the overlapping of emission bands from two different triplet excited states. This effect is also observed for *fac*-**3cd**, although in this case a thpy-centred emission is not clearly distinguishable, probably because of its low intensity.

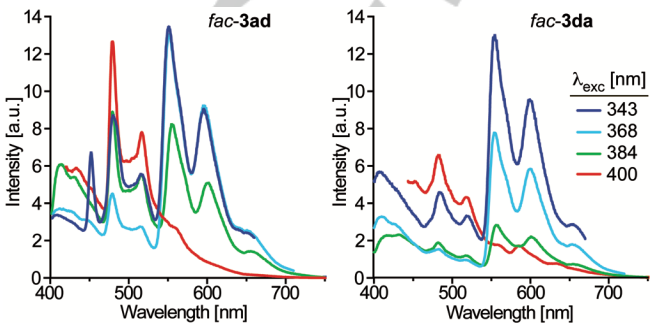

Figure 4. Emission spectra of complexes *fac*-**3ad** and **3da** in PrCN glass at 77 K obtained at different excitation wavelengths.

The observation of a secondary phosphorescent emission from the heteroleptic piq complexes must necessarily be a consequence of relatively low internal conversion rates from higher-lying tpy-, pq- or thpy-centred triplet states to the lowest, piq-centred triplet state, possibly because of weak electronic coupling via the metal dπ orbitals and poor vibrational relaxation, which is less efficient at low temperatures or in rigid media. In agreement with this, the secondary emission is more intense for the complexes with a higher energy difference between the C^N- and C'^N'-centred triplet excited states (*fac*-**3ad** and **3da**), which, according to the energy gap law, must lead to a smaller vibrational overlap between these states. Radiative transitions from the second triplet state may thus become competitive. A relatively inefficient radiative decay from the ^{3}LC(piq) state may also contribute to make the secondary phosphorescence visible. In addition, the above presented data suggest that the population of the emissive ^{3}LC(tpy) state in complexes *fac*-**3ad** and **3da** may preferentially occur via intersystem crossing from ^{1}LC(tpy) states, implying slow internal conversion within the singlet manifold, and from low-lying ^{1}LLCT states. Dual phosphorescence in coordination complexes is rare because internal conversion to the lowest triplet is usually very fast,[41] although it has been observed for certain heteroleptic Ir(III) complexes bearing heteroaromatic ligands of very different π-π* energy gaps.[42–44]

Electrochemistry

For a complete characterization, the redox properties of the new complexes were investigated using cyclic voltammetry in MeCN solution. The potentials of the most important redox processes and highest occupied/lowest unoccupied molecular orbital (HOMO/LUMO) energy estimations are given in Table 2. The previously reported data for *fac*-**3aa**[13] are included for comparison. The complete data and voltammograms are presented in the Supporting Information. While oxidation

processes are not observed for the pq derivatives *fac*-**3ba** and **3bd** within the accessible potential range, the rest of complexes give an irreversible oxidation peak in the range from 1.87 to 2.08 V *vs.* SCE, which is partially overlapped by the solvent discharge. An inspection of these data indicates that the HOMO energy is affected by all of the cyclometalated ligands, yet they allow to extract the following sequence of increasing ligand π-orbital energies: pq (*fac*-**3ba**, **3bd**) < tpy (*fac*-**3aa**) < piq (*fac*-**3ad**, **3da**, **3dd**) < thpy (*fac*-**3ca**, **3cd**). The first reduction peak falls in the range –1.36 to –1.72 V *vs.* SCE and is irreversible in all cases. The observed reduction potentials and the calculated LUMO energies suggest that this orbital is mainly localized on the ligand with the lowest π* orbital, namely pq (*fac*-**3ba**), piq (*fac*-**3ad**, **3bd**, **3cd**, **3da**, **3dd**), thpy (*fac*-**3ca**) or tpy (*fac*-**3aa**). Additional reduction processes are observed at more negative potentials, some of which are reversible or quasi-reversible, probably involving cyclometalated Pt(II) complexes produced as a consequence of the previous irreversible reduction(s) (Table S4, Supporting Information).

Table 2. Electrochemical data[a] and HOMO/LUMO energy estimations[b] for complexes *fac*-**3**.

Complex	$E_{p,a}$[c]	$E_{p,c}$[d]	E_{HOMO}	E_{LUMO}	$\Delta E_{HOMO-LUMO}$
fac-**3aa**	2.03	–1.87	–6.53	–2.97	3.56
fac-**3ad**	2.07	–1.45	–6.49	–3.41	3.08
fac-**3ba**	—[e]	–1.37	—	–3.44	—
fac-**3bd**	—[e]	–1.36	—	–3.44	—
fac-**3ca**	1.87	–1.72	–6.30	–3.12	3.18
fac-**3cd**	1.88	–1.41	–6.36	–3.41	2.95
fac-**3da**	2.08	–1.42	–6.47	–3.41	3.06
fac-**3dd**	2.05	–1.40	–6.46	–3.44	3.02

[a] In V *vs.* SCE, measured in 0.1 M $(Bu_4N)PF_6$ anhydrous MeCN solution at 100 mV s^{-1}. [b] In eV; estimated from the onset values of the oxidation and reduction waves referenced against Fc^+/Fc (0.40 V *vs.* SCE in MeCN), using a formal potential of 5.1 eV for the Fc^+/Fc couple in the Fermi scale.[45] [c] Irreversible anodic peak potential. [d] First irreversible cathodic peak potential. [e] Outside solvent window.

Computational study

DFT and TDDFT calculations were performed for the new *fac*-**3** complexes at the B3LYP/(6-31G**+LANL2DZ) level considering solvent effects (CH_2Cl_2). Full details are given in the Supporting Information. The frontier molecular orbitals are mainly composed of π or π* orbitals from the individual C^N and/or C'^N' ligands with little metal character. The energies of the ligand-based HOMOs or LUMOs (Figure S45, Supporting Information) follow the sequences tpy (*fac*-**3ba**) < piq (*fac*-**3ad**, **3bd**, **3da**, **3dd**) < thpy (*fac*-**3ca**) or piq (*fac*-**3ad**, **3bd**, **3cd**, **3da**, **3dd**) < pq (*fac*-**3ba**) < thpy (*fac*-**3ca**), respectively, in agreement with the electrochemical results.

The TDDFT results show that the most intense singlet excitations are predominantly LC in character. Their predicted energies are compatible with the experimental observations, with no significant variations for each ligand along the series (360-370 nm for piq, 336-339 for thpy, 338-340 nm for pq and 315-317 nm for tpy). Excitations of mainly LLCT character are also predicted, which, in some cases, become the lowest-energy singlet excitations; these transitions have very low oscillator strengths, indicating that the coupling between orbitals localized on different ligands is very weak, probably because of the very low metal orbital contribution. In the heteroleptic piq complexes, the lowest LLCT excitations involve transitions to π*(piq) orbitals, which constitute the LUMO. The heteroleptic complexes present two almost degenerate triplet excitations at the ground-state geometry involving the $Pt(C^N)_2$ fragment and a third one centred on the C'^N' ligand (Figure 5); as expected, the first triplet involves the ligand with the lowest π-π* transition energy. Complex *fac*-**3dd** presents three almost degenerate triplet excitations centred on the piq ligands.

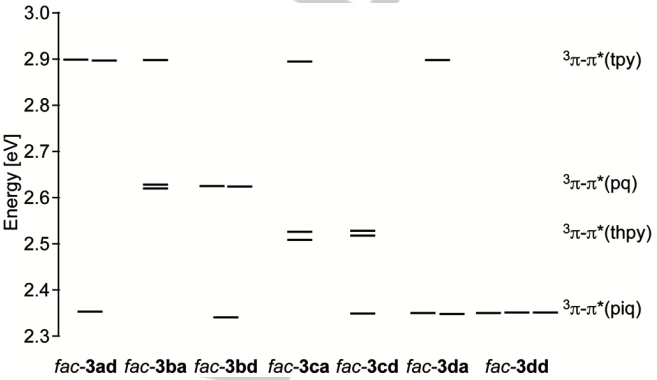

Figure 5. Energy diagram showing the three lowest triplet excitations at the ground-state geometry for complexes *fac*-**3**.

Geometry optimizations of the lowest triplet (T_1) were carried out for all the studied cations. The computed electronic energies with respect to the ground state (adiabatic energy differences) are 2.56 eV (484 nm, *fac*-**3ba**), 2.36 eV (525 nm, *fac*-**3ca**) or 2.18-2.20 eV (562-568 nm, piq-centred states), which are in good agreement with the observed lowest-energy phosphorescent emissions. The spin density distributions (Figure S46, Supporting Information) correspond to an essentially π-π* transition within a single ligand (pq, thpy or piq) with a small contribution from metal orbitals (natural spin densities on the Pt atom in the range 0.011–0.020), which indicate a certain degree of MLCT admixture into the relaxed ^{3}LC state.[14,15] Attempts to optimize the lowest ^{3}LC(tpy) state in *fac*-**3ad** (T_2) were unsuccessful due to variational collapse to the ^{3}LC(piq) state, but succeeded for *fac*-**3da** (T_3). The calculated adiabatic energy difference with respect to the ground state is 2.78 eV (446 nm), which matches the secondary phosphorescent emission.

Conclusion

A stereoselective method for the synthesis of homo- and heteroleptic facial tris-cyclometalated Pt(IV) complexes has been developed, which allows the cyclometalation of 2-arylpyridines of variable π-π* transition energies and opens the way to an extensive modulation of the electrochemical and photophysical properties of this kind of complexes through ligand variation. The isolation and characterization of intermediate complexes bearing a chelating diazenide ligand has been achieved for the first time.

The new complexes exhibit ^{3}LC emissions in fluid solution at 298 K, which involve the ligand with the lowest π-π* energy gap in the heteroleptic derivatives. In rigid media at room or low temperatures, the heteroleptic complexes bearing the piq ligand show fluorescent and dual phosphorescent emissions arising from a ^{1}LC(piq) excited state and two ^{3}LC excited states involving

piq and the other cyclometalated ligand. The observation of a secondary phosphorescence is mainly attributable to slow internal conversion within the triplet manifold, possibly because of weak electronic coupling and poor vibrational relaxation. Tris-cyclometalated Pt(IV) complexes have thus been demonstrated as suitable for the design of multi-emissive species and further developments may lead to practical application as white light-emitting materials.

Experimental Section

General considerations and materials: Unless otherwise noted, all reactions in solution were carried out at room temperature using extra-dry MeOH or MeCN and flame-dried glassware under an N_2 atmosphere. Synthesis grade Et_2O and CH_2Cl_2 were degassed and dried using a Pure Solv MD-5 solvent purification system from Innovative Technologies, Inc. Other solvents were used as received. The visible-light irradiation source was a commercial 3.45 W blue LED strip fixed on the inner wall of a 500 mL crystallising dish, as previously described.[19] The compounds *cis*-[Pt(C^N)$_2$] [C^N = tpy (**1a**), thpy (**1c**) or piq (**1d**)],[19] 5-methyl-2-(2-pyridyl)benzenediazonium tetrafluoroborate,[22] 5-methyl-2-(2-pyridyl)benzenediazonium tetraphenylborate[46] and 2-(1-isoquinolinyl)benzenediazonium tetrafluoroborate[22] were prepared following published procedures. Complex *cis*-[Pt(pq)$_2$] (**1b**) has not been previously reported and its preparation is given in the Supporting Information.

Spectroscopic and analytical methods: NMR spectra were recorded on a Bruker Avance 600 MHz spectrometer at 298 K. Chemical shifts are referenced to residual signals of non-deuterated solvents and are given in ppm downfield from tetramethylsilane. Elemental analyses were carried out with a LECO CHNS-932 microanalyzer. High-resolution electrospray ionization mass spectra (ESI-MS) were recorded on an Agilent 6220 Accurate-Mass time-of-flight LC/MS. UV-vis absorption spectra were recorded on a Perkin-Elmer Lambda 750S spectrophotometer. Excitation and emission spectra were recorded on a Jobin Yvon Fluorolog 3-22 spectrofluorometer equipped with double-grating monochromators and a TBX-04 photomultiplier. Measurements in solution were carried out using 10 mm quartz fluorescence cells (298 K) or 5 mm quartz NMR tubes (77 K). For the low-temperature measurements, a liquid nitrogen Dewar with quartz windows was employed. The photophysical data in PMMA thin films were measured using quartz slides as sample holders. Lifetimes were measured using an IBH FluoroHub controller in MCS mode and the Fluorolog's FL-1040 phosphorimeter pulsed xenon lamp as excitation source; the estimated uncertainty is ±10% or better. Emission quantum yields (Φ) were measured using a Hamamatsu C11347 Absolute PL Quantum Yield Spectrometer; the estimated uncertainty is ±5% or better. Emission data were obtained under rigorous exclusion of oxygen, by bubbling argon through the solutions for 30 min or placing the PMMA films under argon.

Synthesis of [Pt(tpy)$_2$(N$_2$tpy)]BPh$_4$ (2aa-BPh$_4$): To a suspension of **1a** (51 mg, 0.10 mmol) in MeOH (2 mL) was added 5-methyl-2-(2-pyridyl)benzenediazonium tetraphenylborate (49 mg, 0.09 mmol) and the resultant dark red solution was stirred for 15 min. The addition of Et_2O (20 mL) led to the precipitation of an orange solid, which was collected by filtration, washed with Et_2O (3 × 2 mL) and vacuum-dried to give **2aa-BPh$_4$**. Yield: 87 mg, 92 %. ^{1}H NMR (600 MHz, CD_2Cl_2): δ=8.13 (d, *J*=8.2 Hz, 1H), 7.95 (d, *J*=7.9 Hz, 1H), 7.88 (t, *J*=7.7 Hz, 1H), 7.76 (m, 3H), 7.70 (t, *J*=7.8 Hz, 1H), 7.53 (t, *J*=6.7 Hz, 2H), 7.47–7.37 (m, 3H), 7.34–7.22 (m, 10H), 7.04–6.90 (m, 11H), 6.84–6.76 (m, 5H), 6.66 (t, *J*=6.5 Hz, 1H), 6.59 (s with satellites $J_{H,Pt}$=43.3 Hz, 1H), 6.55 (s, 1H), 2.48 (s, 3H), 2.25 (s, 3H), 2.13 ppm (s, 3H); ^{13}C {^{1}H} APT NMR (150.8 MHz, CD_2Cl_2): δ=165.1 (C), 164.8 (C), 164.4 (C), 164.1 (C), 161.8 (C), 161.7 (C), 157.7 (C), 151.2 (CH), 149.4 (CH), 148.2 (C), 147.0 (CH), 145.0 (C), 143.8 (C), 143.4 (C), 143.3 (C), 141.4 (CH), 141.3 (CH), 139.7 (CH), 138.5 (C), 138.2 (C), 136.5 (CH), 135.3 (CH), 135.0 (CH), 130.0 (CH), 129.6 (CH), 129.1 (CH), 127.6 (CH), 127.0 (CH), 126.2 (CH), 125.4 (CH), 125.0 (CH), 124.3 (CH), 124.1 (CH), 123.8 (CH), 122.3 (CH), 121.7 (CH), 120.4 (CH), 22.4 (CH_3), 22.1 (CH), 21.1 ppm (CH); elemental analysis calcd (%) for $C_{60}H_{50}BN_5Pt$: C 68.83, H 4.81, N 6.69; found: C 69.00, H 4.85, N 6.59; HRMS (ESI+, m/z) calcd for $C_{36}H_{30}N_5Pt$ [M]$^+$: 727.2149; found: 727.2142.

Synthesis of [Pt(thpy)$_2$(N$_2$tpy)]BF$_4$ (2ca): To a suspension of **1c** (51 mg, 0.10 mmol) in MeOH (2 mL) was added 5-methyl-2-(2-pyridyl)benzenediazonium tetraphenylborate (49 mg, 0.09 mmol) and the resultant dark red solution was stirred for 15 min. The addition of Et_2O (20 mL) led to the precipitation of an orange solid, which was collected by filtration, washed with Et_2O (3 × 2 mL) and vacuum-dried to give **2ca**. Yield: 87 mg, 91%. ^{1}H NMR (400 MHz, CD_3CN): δ 8.10 (td, *J*=7.7, 1.6 Hz, 2H), 8.02–7.86 (m, 4H), 7.86–7.74 (m, 3H), 7.59–7.45 (m, 3H), 7.44–7.36 (m, 2H), 7.36–7.21 (m, 3H), 6.99 (ddd, *J*=7.4, 5.7, 1.4 Hz, 1H), 6.82 (ddd, *J*=7.4, 5.7, 1.4 Hz, 1H), 6.64 (s, 1H), 6.35 (d, $J_{H,Pt}$=17.6 Hz, $J_{H,H}$=4.9 Hz, 1H), 2.23 ppm (s, 3H); elemental analysis calcd (%) for $C_{30}H_{22}BF_4N_5PtS_2$: C 45.12, H 2.78, N 8.77, S 8.03; found: C 45.05, H 2.74, N 8.80, S 7.98; HRMS (ESI+, m/z) calcd for $C_{30}H_{22}N_5S_2Pt$ [M]$^+$: 711.0964; found: 711.0928.

Visible-light irradiation of diazenide intermediates: To a suspension of complex **1** (0.10 mmol) in MeCN (2 mL) was added the diazonium salt (0.10 mmol) and the resultant dark red solution was stirred and irradiated with blue LEDs for 24 h, whereupon the colour changed to dark brown. The addition of Et_2O (20 mL) led to the precipitation of an orange solid, which was collected by filtration and vacuum-dried. As deduced from ^{1}H NMR data, this solid was a mixture of *fac*- and *mer*-**3** isomers in variable proportions (Figures S12-S15), except for the homoleptic piq complex, which was obtained exclusively as the *fac* isomer (*fac*-**3dd**) and purified by chromatography on silica gel using a $CHCl_3$/MeOH mixture (15:1) as the eluent.

General procedure for the synthesis of facial tris-cyclometalated Pt(IV) complexes: To a suspension of the appropriate complex **1** (0.10 mmol) in MeCN or MeOH (2 mL) was added 5-methyl-2-(2-pyridyl)benzenediazonium tetrafluoroborate or 2-(1-isoquinolinyl)benzenediazonium tetrafluoroborate (0.10 mmol) and the resultant dark red solution was stirred for 15 min. The addition of Et_2O (20 mL) led to the precipitation of an orange solid, which was collected by filtration, transferred to a vial and heated at 150 °C in a silicone oil bath for 3 h. The resultant solid was chromatographed on silica gel using a $CHCl_3$/MeOH mixture (15:1) as the eluent and crystallized from CH_2Cl_2/Et_2O to give the corresponding complex *fac*-**3**.

***fac*-[Pt(tpy)$_3$]BF$_4$ (*fac*-3aa):** White solid. ^{1}H NMR (600 MHz, CD_2Cl_2): δ=8.10 (d, *J*=8.3 Hz, 3H), 8.05–7.98 (m, 3H), 7.71 (d, *J*=8.0, Hz, 3H), 7.56 (d, *J*=5.4 Hz, 3H), 7.28 (t, *J*=7.7 Hz, 3H), 7.10 (d, *J*=8.0 Hz, 3H), 6.45 (s with satellites $J_{H,Pt}$=46.4 Hz, 3H), 2.16 ppm (s, 9H); ^{13}C {^{1}H} APT NMR (150.8 MHz, CD_2Cl_2): δ=163.0 ($J_{C,Pt}$=49.9 Hz, C), 146.6 (CH), 143.7 ($J_{C,Pt}$=49.6 Hz, C), 142.1 (C), 141.3 (CH), 138.7 (C), 133.1 ($J_{C,Pt}$=50.6 Hz, C), 127.4 (CH), 126.1 ($J_{C,Pt}$=33.0 Hz, C), 125.1 (CH), 121.5 (CH), 22.1 ppm (CH_3); elemental analysis calcd for $C_{36}H_{30}BF_4N_3Pt$: C 54.97, H 3.84, N 5.34; found: C 54.63, H 3.83, N 5.20; HRMS (ESI+, m/z) calcd for $C_{36}H_{30}N_3Pt$ [M]$^+$: 699.2087; found: 699.2132.

***fac*-[Pt(tpy)$_2$(piq)]BF$_4$ (*fac*-3ad):** Pale yellow solid.^{1}H NMR (600 MHz, CD_2Cl_2): δ=8.99 (d, *J*=8.7 Hz, 1H), 8.36 (d, *J*=8.0 Hz, 1H), 8.11 (d, *J*=8.2 Hz, 2H), 8.08–8.00 (m, 3H), 7.93 (t, *J*=7.7 Hz, 1H), 7.89 (t, *J*=7.7 Hz, 1H), 7.72 (dd, *J*=15.3, 8.4 Hz), 7.67 (d, *J*=6.2 Hz, 1H), 7.58 (d, *J*=4.9 Hz, 1H), 7.47 (m, 2H), 7.38 (t, *J*=6.8 Hz, 1H), 7.30 (t, *J*=6.8 Hz, 1H), 7.19 (t, *J*=6.8 Hz, 1H), 7.14 (t, *J*=6.8 Hz, 1H), 7.11 (d, *J*=8.5 Hz, 1H), 7.06 (d, *J*=8.5 Hz, 1H), 6.83 (d with satellites, $J_{H,Pt}$=48.4 Hz, $J_{H,H}$=7.5 Hz, 1H), 6.47 (s with satellites, *J*=46.5 Hz, 1H), 6.40 (s with satellites, $J_{H,Pt}$=46.5 Hz, 1H), 2.17 (s, 3H), 2.11 ppm (s, 3H); ^{13}C {^{1}H} APT NMR (150.8 MHz, CD_2Cl_2): δ=165.4 (C), 164.0 (C), 164.0 (C), 147.7 (CH), 147.5 (CH), 144.9 (C), 144.8 (C), 144.6 (C), 144.0 (C), 143.7 (C), 143.1 (C), 142.4 (CH), 139.9

(C), 139.7 (C), 138.5 (CH), 134.5 (CH), 134.1 (CH), 134.0 (CH), 134.0 (CH), 133.0 ($J_{C,Pt}$=33.6 Hz, CH), 131.4 (CH), 129.6 (CH), 128.8 (CH), 128.5 (CH), 128.4 (CH), 128.2 (C), 127.2 (CH), 127.13 (CH), 127.07 (CH), 126.2 (CH), 126.1 (CH), 125.2 (CH), 122.6 ($J_{C,Pt}$=14.7 Hz, CH), 23.13 (CH_3), 23.09 ppm (CH_3); elemental analysis calcd (%) for $C_{39}H_{30}BF_4N_3Pt$: C 56.95, H 3.68, N 5.11; found: C 57.11, H 3.68, N 5.06; HRMS (ESI+, m/z) calcd for $C_{39}H_{30}N_3Pt$ $[M]^+$: 735.2087; found: 735.2098.

***fac*-[Pt(pq)$_2$(tpy)]BF$_4$ (*fac*-3ba):** Pale brown solid. ^{1}H NMR (600 MHz, CD_2Cl_2): δ=8.62 (d, *J*=8.8 Hz, 1H), 8.48 (d, *J*=8.8 Hz, 1H), 8.42 (d, *J*=8.9 Hz, 1H), 8.27 (d, *J*=8.8 Hz, 1H), 8.12–8.06 (m, 1H), 8.02–7.90 (m, 5H), 7.84 (d, *J*=9.0, 1H), 7.81 (d, *J*=5.4 Hz, 1H), 7.54–7.47 (m, 2H), 7.45 (t, *J*=8.0, 1H), 7.37 (t, *J*=7.6 Hz, 1H), 7.30 (t, *J*=7.6 Hz, 1H), 7.27–7.21 (m, 2H), 7.20-7.16 (m, 1H), 7.08–6.99 (m, 2H), 6.50 (d with satellites, $J_{H,Pt}$=41.9 Hz, $J_{H,H}$=7.9 Hz, 1H), 6.48 (d with satellites, $J_{H,Pt}$=53.5 Hz, $J_{H,H}$=7.3 Hz), 6.28 (s with satellites, $J_{H,Pt}$=47.1 Hz, 1H), 2.07 ppm (s, 3H); ^{13}C{^{1}H} APT NMR (150.8 MHz, CD_2Cl_2): δ=165.4 (C), 164.3(C), 162.8 (C), 147.1 (CH), 146.7 (CH), 146.6 (C), 144.2 (C), 143.7 (C), 142.5 (CH), 142.0 (CH), 141.4 (C), 138.0 (C), 133.6 ($J_{C,Pt}$=64.5 Hz, CH), 132.8 (CH), 132.7 (CH), 132.6 (CH), 132.4 (CH), 131.4 ($J_{C,Pt}$=64.5 Hz, CH), 130.6 ($J_{C,Pt}$=45.2 Hz, CH), 130.2 (CH), 130.0 (CH), 129.4 (C), 129.1 (C), 128.7 (CH), 128.6 (CH), 128.0 (CH), 127.8 (CH), 127.2 (CH), 126.7 (CH), 126.1 ($J_{C,Pt}$=34.4 Hz, CH), 125.6 (CH), 125.4 (CH), 124.6 (CH), 121.9 (CH), 119.7 (CH), 119.5 (CH), 22.1 ppm (CH_3); elemental analysis calcd (%) for $C_{42}H_{30}BF_4N_3Pt{\cdot}0.25CH_2Cl_2$: C 57.68, H 3.49, N 4.78; found: C 57.89, H 3.37, N 4.66; HRMS (ESI+, m/z) calcd for $C_{42}H_{30}N_3Pt$ $[M]^+$: 771.2087; found: 771.2070.

***fac*-[Pt(pq)$_2$(piq)]BF$_4$ (*fac*-3bd):** Brown solid. ^{1}H NMR (600 MHz, CD_2Cl_2): δ=8.72 (d, *J*=8.8 Hz, 1H), 8.62 (d, *J*=8.8 Hz, 1H), 8.47 (d, *J*=8.8 Hz, 1H), 8.42 (d, *J*=8.9 Hz, 1H), 8.27 (d, *J*=8.8 Hz, 1H), 8.12–8.04 (m, 2H), 8.02–7.95 (m, 3H), 7.95–7.84 (m, 3H), 7.82 (ddd, *J*=8.5, 6.9, 1.4 Hz, 1H), 7.77–7.72 (m, 1H), 7.61 (d, *J*=6.3 Hz, 1H), 7.46 (t, *J*=7.9 Hz, 1H), 7.37 (t, *J*=7.9 Hz, 1H), 7.34–7.28 (m, 2H), 7.23 (t, *J*=7.9 Hz, 1H), 7.19 (d, *J*=9.0 Hz, 1H), 7.05–6.95 (m, 4H), 6.82 (t, *J*=7.9 Hz, 1H), 6.63 (dd with satellites, $J_{H,Pt}$=49.1 Hz, $J_{H,H}$=7.9, 1.0 Hz), 6.55 (dd with satellites, $J_{H,Pt}$=52.5 Hz, $J_{H,H}$=8.1, 0.8 Hz), 6.51 ppm (dd with satellites, $J_{H,Pt}$=45.3 Hz, $J_{H,H}$=7.9, 0.9 Hz); ^{13}C {^{1}H} APT NMR (150.8 MHz, CD_2Cl_2): δ=165.4 (C), 164.4 (C), 164.2 (C), 146.9 (CH), 146.4 (C), 143.7 (C), 143.5 (C), 143.1 (C), 142.5 (CH), 142.4 (C), 142.3 (C), 141.9 (CH), 141.8 (CH), 138.5 (C), 138.1 (CH), 133.6 (CH), 133.5 ($J_{C,Pt}$=63.6 Hz, CH), 133.0 ($J_{C,Pt}$=63.6 Hz, CH), 132.8 (CH), 132.7 (CH), 132.5 ($J_{C,Pt}$=44.5 Hz, CH), 132.2 (CH), 131.7 ($J_{C,Pt}$=33.8 Hz, CH), 131.2 ($J_{C,Pt}$=58.2 Hz, CH), 130.6 (CH), 130.5 ($J_{C,Pt}$=44.5 Hz, CH), 130.1 (CH), 130.0 (CH), 129.4 (C), 129.1 (C), 128.61 (CH), 128.56 (CH), 128.5 (CH), 128.3 (CH), 127.9 (CH), 127.5 (CH), 127.1 (CH), 126.8 (CH), 126.4 (CH), 125.6 (CH), 124.8 (CH), 124.4 (CH), 119.7 ($J_{C,Pt}$=15.1 Hz, CH), 119.4 ppm ($J_{C,Pt}$=15.1 Hz, CH); elemental analysis calcd (%) for $C_{45}H_{30}BF_4N_3Pt$: C 60.41, H 3.38, N 4.70; found: C 60.28, H 3.32, N 4.65; HRMS (ESI+, m/z) calcd for $C_{45}H_{30}N_3Pt$ $[M]^+$: 807.2087; found: 807.2093.

***fac*-[Pt(thpy)$_2$(tpy)]BF$_4$ (*fac*-3ca):** Pale yellow solid. ^{1}H NMR (CD_2Cl_2, 600 MHz): δ=8.12–8.03 (m, 2H), 7.97 (m, 2H), 7.79–7.71 (m, 3H), 7.71–7.66 (m, 2H), 7.60–7.54 (d with satellites, $J_{H,Pt}$=18.1 Hz, $J_{H,H}$=6.4 Hz, 1H), 7.44 (d with satellites, $J_{H,Pt}$=14.6, $J_{H,H}$=5.2 Hz, 1H), 7.42 (d with satellites, $J_{H,Pt}$=14.6, $J_{H,H}$=5.2 Hz, 1H), 7.40–7.34 (m, 1H), 7.25 (t, *J*=6.4 Hz, 1H), 7.22 (t, *J*=6.4 Hz, 1H), 7.10 (d, *J*=7.6 Hz, 1H), 6.39 (s with satellites, $J_{H,Pt}$=47.0 Hz, 1H), 6.33 (d with satellites, $J_{H,Pt}$=18.1 Hz, $J_{H,H}$=5.3 Hz, 1H), 6.30 (d with satellites, $J_{H,Pt}$=18.1 Hz, $J_{H,H}$=5.3 Hz, 1H), 2.19 ppm (s, 3H); ^{13}C {^{1}H} APT NMR (150.8 MHz, CD_2Cl_2): δ=162.9 ($J_{C,Pt}$=53.0, C), 158.9 ($J_{C,Pt}$=40.4 Hz, C), 158.3 ($J_{C,Pt}$=40.4 Hz, C), 147.5 (CH), 147.3 (CH), 143.6 ($J_{C,Pt}$=55.5 Hz, C), 141.9 (CH), 141.9 (CH), 141.7 (CH), 141.4 (C), 133.9 ($J_{C,Pt}$=46.8 Hz, CH), 131.3 ($J_{C,Pt}$=66.5 Hz, CH), 130.6 ($J_{C,Pt}$=73.8 Hz, CH), 129.8 ($J_{C,Pt}$=80.1 Hz, CH), 127.7 (CH), 126.0 ($J_{C,Pt}$=33.3 Hz, CH), 125.5 (CH), 123.9 (CH), 123.6 (CH), 121.4 CH), 120.8 (CH), 120.6 (CH), 22.1 ppm (CH_3); elemental analysis calcd (%) for $C_{30}H_{22}BF_4N_3PtS_2$: C 46.76, H 2.88, N 5.45, S 8.32; found: C 46.73, H 2.73, N 5.16, S 8.24; HRMS (ESI+, m/z) calcd for $C_{30}H_{22}N_3PtS_2$ $[M]^+$: 683.0903; found: 683.0892.

***fac*-[Pt(thpy)$_2$(piq)]BF$_4$ (*fac*-3cd):** Yellow solid. ^{1}H NMR (600 MHz, CD_2Cl_2): δ=8.98 (d, *J*=8.7 Hz, 1H), 8.35 (d, *J*=8.29, 1H), 8.07 (d, *J*=8.2 Hz, 1H), 8.01 (t, *J*=7.9 Hz, 1H), 7.96 (q, *J*=7.9 Hz, 2H), 7.90 (t, *J*=8.2 Hz, 1H), 7.80–7.74 (m, 3H), 7.72–7.63 (m, 2H), 7.46 (d with satellites, $J_{H,Pt}$=14.2 Hz, $J_{H,H}$=5.6 Hz, 1H), 7.44–7.36 (m, 3H), 7.28 (m, 1H), 7.18 (m, 1H), 7.13 (m, 1H), 6.78 (dd with satellites, $J_{H,Pt}$=49.1 Hz, $J_{H,H}$=7.8, 1.1 Hz, 1H), 6.33 (d with satellites, $J_{H,Pt}$=18.5 Hz, $J_{H,H}$=4.8 Hz, 1H), 6.26 ppm (d with satellites, $J_{H,Pt}$=18.5 Hz, $J_{H,H}$=4.8 Hz, 1H); ^{13}C {^{1}H} APT NMR (150.8 MHz, CD_2Cl_2): δ=163.7 ($J_{C,Pt}$=53.3 Hz, C), 158.4 ($J_{C,Pt}$=37.3 Hz, C), 157.7 ($J_{C,Pt}$=37.3 Hz, C), 146.7 (CH), 142.8 (C), 141.5 (CH), 141.4 (CH), 138.4 (C), 137.5 (CH), 136.2 (C), 133.2 (CH), 133.1 (CH), 132.2 ($J_{C,Pt}$=57.6 Hz, CH), 131.2 ($J_{C,Pt}$=32.1 Hz, CH), 130.9 ($J_{C,Pt}$=69.1 Hz, CH), 130.1 (CH), 130.0 (CH), 129.8 (CH), 129.3 ($J_{C,Pt}$=80.1 Hz, CH), 128.2 (CH), 127.1 (CH), 126.4 ($J_{C,Pt}$=20.1 Hz, C), 125.9 (CH), 124.1 (CH), 123.4 (CH), 123.1 (CH), 120.3 (CH), 120.2 ppm (CH); elemental analysis calcd (%) for $C_{33}H_{22}BF_4N_3PtS_2$: C 49.14, H 2.75, N 4.96, S 7.95; found: C 48.99, H 2.71, N 4.92, S 7.63; HRMS (ESI+, m/z) calcd for $C_{33}H_{22}N_3PtS_2$ $[M]^+$: 719.0903; found: 719.0905.

***fac*-[Pt(piq)$_2$(tpy)]BF$_4$ (*fac*-3da):** Yellow solid. ^{1}H NMR (600 MHz, CD_2Cl_2): δ=9.00 (t, *J*=8.8 Hz, 2H), 8.36 (dd, *J*=17.2, 8.8 Hz, 1H), 8.13 (d, *J*=8.39 Hz, 1H), 8.07–7.84 (m, 7H), 7.72 (d, *J*=8.38 Hz, 1H), 7.69 (d, *J*=6.1 Hz, 1H), 7.58 (d, *J*=6.1 Hz, 1H), 7.52 (d, *J*=5.3 Hz, 1H), 7.49 (d, *J*=6.1 Hz, 1H), 7.42–7.37 (m, 2H), 7.39 (m, 1H), 7.34 (m, 1H), 7.21 (m, 1H), 7.15 (m, 1H), 7.12–7.06 (m, 1H), 6.84 (dd with satellites, $J_{H,Pt}$=48.5 Hz, $J_{H,H}$=7.8, 1.0 Hz, 1H), 6.80 (dd with satellites, $J_{H,Pt}$=48.9 Hz, $J_{H,H}$=7.8, 1.0 Hz, 1H), 6.44 (s with satellites, $J_{H,Pt}$=47.2 Hz, 1H), 2.12 ppm (s, 3H); ^{13}C{^{1}H} APT NMR (150.8 MHz, CD_2Cl_2): δ=164.5 ($J_{C,Pt}$=48.6 Hz, C), 164.4 ($J_{C,Pt}$=48.6 Hz, C), 163.0 ($J_{C,Pt}$=48.6 Hz, C), 146.6 (CH), 144.1 (C), 143.9 (C), 143.6 (C), 143.02 (C), 142.99 (C), 142.6 (C), 141.5 (CH), 138.9 (C), 138.8 (C), 137.6 (CH), 137.5 (CH), 133.53 (CH), 133.51 (CH), 133.14 (CH), 132.98 (CH), 132.9 (CH), 132.8 (CH), 132.0 ($J_{C,Pt}$=33.1 Hz, CH), 131.9 ($J_{C,Pt}$=33.3 Hz, CH), 130.5 (CH), 130.4 (CH), 128.6 (CH), 128.5 (CH), 127.8 (CH), 127.5 (CH), 127.2 (C), 127.1 (C), 126.2 (CH), 126.1 (CH), 126.0 (CH), 125.2 (CH), 124.3 (CH), 124.2 (CH), 121.7 (CH), 22.1 ppm (CH_3); elemental analysis calcd (%) for $C_{42}H_{30}BF_4N_3Pt$: C 58.75, H 3.52, N 4.89; found: C 58.66, H 3.54, N 4.75; HRMS (ESI+, m/z) calcd for $C_{42}H_{30}N_3Pt$ $[M]^+$: 771.2087; found: 771.2100.

***fac*-[Pt(piq)$_3$]BF$_4$ (*fac*-3dd):** Yellow solid. ^{1}H NMR (600 MHz, CD_2Cl_2): δ=8.99 (d, *J*=8.6 Hz, 3H), 8.36 (d, *J*=8.3 Hz, 3H), 8.00 (d, *J*=7.9 Hz, 3H), 8.03-7.83 (m, 6H), 7.62 (d, *J*=6.5 Hz, 3H), 7.49 (d, *J*=6.7 Hz, 3H), 7.35 (t, *J*=7.3 Hz, 3H), 7.10 (m, 3H), 6.84 ppm (dd with satellites, $J_{H,Pt}$=48.5 Hz, $J_{H,H}$=7.9, 1.2 Hz, 3H); ^{13}C{^{1}H} APT NMR (150.8 MHz, CD_2Cl_2): δ=164.5 ($J_{C,Pt}$=40.6 Hz, C), 144.0 (C), 143.1 (C), 138.9 (C), 137.5 (CH), 133.6 (CH), 132.9 (CH), 132.7 ($J_{C,Pt}$=47.01 Hz, CH), 132.0 ($J_{C,Pt}$=33.2 Hz, CH), 130.5 (CH), 128.6 (CH), 127.8 (CH), 127.3 (C), 126.2 (CH), 124.3 ppm (CH); elemental analysis calcd (%) for $C_{45}H_{30}BF_4N_3Pt$: C 60.41, H 3.38, N 4.70; found: C 60.11, H 3.24, N 4.78; HRMS (ESI+, m/z) calcd for $C_{45}H_{30}N_3Pt$ $[M]^+$: 807.2087; found: 807.2089.

X-Ray structure determinations: Single crystals suitable for X-ray diffraction were grown by slow liquid diffusion of *n*-pentane into a solution of the complex (**2aa-BPh$_4$**) or a mixture of *fac*-**3dd** and $NaBPh_4$ (*fac*-**3dd-BPh$_4$**) in CH_2Cl_2. Numerical details are presented in the Supporting Information (Table S1). The data were collected on a Bruker D8 QUEST diffractometer with monochromated Mo-*K*α radiation performing φ and ω scans. The structures were solved by dual methods[47] and refined anisotropically on F^2 using the program SHELXL-2018 (G. M. Sheldrick, University of Göttingen).[48] Methyl hydrogens were included as part of rigid idealized methyl groups allowed to rotate but not tip; other hydrogens were included using a riding model. *Special features of refinement:* In *fac*-**3dd-BPh$_4$**, there is a poorly resolved region of residual electron density that could not be adequately modelled and therefore the program SQUEEZE,[49] which is part of the PLATON system, was employed to mathematically remove the effects of the solvent; the void volume per cell was 338 Å^3, with a void electron count per cell of 8; this additional solvent

was not taken into account when calculating derived parameters such as the formula weight, because its nature was uncertain.

CCDC 1985915 (**2aa-BPh$_4$**) and CCDC 1985916 (*fac*-**3dd-BPh$_4$**) contain the supplementary crystallographic data for this paper. These data can be obtained free of charge from the Cambridge Crystallographic Data Centre via http://www.ccdc.cam.ac.uk/data_request/cif.

Electrochemical characterization: Cyclic voltammograms were registered with a potentiostat/galvanostat AUTOLAB-100 (Echo-Chemie, Utrecht), employing a three-electrode electrochemical cell equipped with a glassy carbon working electrode (Metrohm, 2 mm diameter), an Ag/AgCl/3 M KCl electrode reference, and a glassy carbon rod counter electrode. The measurements were carried out at 298 K under an argon atmosphere, using degassed 1 mM solutions of the complexes in extra-dry MeCN (Acros Organics) and 0.1 M ($Bu_4N)PF_6$ as the electrolyte. Prior to each experiment, the working electrode was polished with alumina slurry (0.05 μm) and rinsed with water and acetone. The electrodes were activated electrochemically in the background solution by means of several voltammetric cycles at 1 V s^{-1} between –2.7 V and 2.2 V. At the end of each experiment, the reference electrode was checked against the ferrocene/ferricinium redox couple. Potentials are given *vs.* the standard calomel electrode (SCE).

Computational methods: DFT calculations were carried out with the Gaussian 09 package,[50] using the hybrid B3LYP functional[51,52] together with the 6-31G**[53,54] basis set for the light atoms and the LANL2DZ[55] basis set and effective core potential for the Pt atom. All geometry optimizations were carried out without symmetry restrictions, using "tight" convergence criteria and "ultrafine" integration grid. Vertical excitation energies were obtained from TDDFT calculations at the ground-state optimized geometries. Triplet state geometries were obtained through a spin-unrestricted DFT (UB3LYP) optimization, following a previously described strategy.[56] The solvent effect (CH_2Cl_2) was accounted for in all cases by using the integral equation formalism variant of the polarizable continuum solvation model (IEFPCM).[57] All the optimized structures were confirmed as minima on the potential energy surface by performing frequency calculations (zero imaginary frequencies). Natural spin densities were obtained from natural population analyses using the NBO 5.9 program.[58]

Acknowledgements

We thank Fundación Séneca (19890/GERM/15), Ministerio de Economía y Competitividad (CTQ2015-69568-P) and Ministerio de Ciencia, Innovación y Universidades (PGC2018-100719-BI00) for financial support.

Keywords: cyclometalating ligands • electrochemistry • luminescence • photophysics • platinum

[1] V. Balzani, G. Bergamini, S. Campagna, F. Puntoriero, *Top. Curr. Chem.* **2007**, *280*, 1–36.

[2] J. C. Deaton, F. N. Castellano, in *Iridium(III) Optoelectron. Photonics Appl.* (Ed.: E. Zysman-Colman), John Wiley & Sons, Ltd, Chichester, UK, **2017**, pp. 1–69.

[3] F. Heinemann, J. Karges, G. Gasser, *Acc. Chem. Res.* **2017**, *50*, 2727–2736.

[4] S. Monro, K. L. Colón, H. Yin, J. Roque, P. Konda, S. Gujar, R. P. Thummel, L. Lilge, C. G. Cameron, S. A. McFarland, *Chem. Rev.* **2019**, *119*, 797–828.

[5] V. Guerchais, J.-L. Fillaut, *Coord. Chem. Rev.* **2011**, *255*, 2448–2457.

[6] E. D. Cline, S. E. Adamson, S. Bernhard, *Inorg. Chem.* **2008**, *47*, 10378–10388.

[7] M. S. Lowry, J. I. Goldsmith, J. D. Slinker, R. Rohl, R. A. Pascal, G. G. Malliaras, S. Bernhard, *Chem. Mater.* **2005**, *17*, 5712–5719.

[8] C. K. Prier, D. A. Rankic, D. W. C. MacMillan, *Chem. Rev.* **2013**, *113*, 5322–5363.

[9] D. M. Schultz, T. P. Yoon, *Science* **2014**, *343*, 1239176.

[10] M. E. Thompson, P. E. Djurovich, S. Barlow, S. Marder, in *Compr. Organomet. Chem. III* (Eds.: H.C. Robert, D.M.P. Mingos), Elsevier, Oxford, **2007**, pp. 101–194.

[11] L. Xiao, Z. Chen, B. Qu, J. Luo, S. Kong, Q. Gong, J. Kido, *Adv. Mater.* **2011**, *23*, 926–952.

[12] R. D. Costa, E. Ortí, H. J. Bolink, F. Monti, G. Accorsi, N. Armaroli, *Angew. Chem., Int. Ed.* **2012**, *51*, 8178–8211.

[13] F. Juliá, D. Bautista, J. M. Fernández-Hernández, P. González-Herrero, *Chem. Sci.* **2014**, *5*, 1875–1880.

[14] F. Juliá, G. Aullón, D. Bautista, P. González-Herrero, *Chem. Eur. J.* **2014**, *20*, 17346–17359.

[15] F. Juliá, P. González-Herrero, *Dalton Trans.* **2016**, *45*, 10599–10608.

[16] Y. Tamura, Y. Hisamatsu, A. Kazama, K. Yoza, K. Sato, R. Kuroda, S. Aoki, *Inorg. Chem.* **2018**, *57*, 4571–4589.

[17] E. Baranoff, B. F. E. Curchod, J. Frey, R. Scopelliti, F. Kessler, I. Tavernelli, U. Rothlisberger, M. Grätzel, M. K. Nazeeruddin, *Inorg. Chem.* **2012**, *51*, 215–224.

[18] J. H. Seo, I. J. Kim, Y. K. Kim, Y. S. Kim, *Thin Solid Films* **2008**, *516*, 3614–3617.

[19] F. Juliá, P. González-Herrero, *J. Am. Chem. Soc.* **2016**, *138*, 5276–5282.

[20] A. von Zelewsky, A. P. Suckling, H. Stoeckli-Evans, *Inorg. Chem.* **1993**, *32*, 4585–4593.

[21] L. Chassot, A. von Zelewsky, D. Sandrini, M. Maestri, V. Balzani, *J. Am. Chem. Soc.* **1986**, *108*, 6084–6085.

[22] S. Kim, J. Rojas-Martin, F. D. Toste, *Chem. Sci.* **2016**, *7*, 85–88.

[23] A. Tlahuext-Aca, M. N. Hopkinson, C. G. Daniliuc, F. Glorius, *Chem. Eur. J.* **2016**, *22*, 11587–11592.

[24] L. Huang, M. Rudolph, F. Rominger, A. S. K. Hashmi, *Angew. Chem., Int. Ed.* **2016**, *55*, 4808–4813.

[25] L. Huang, F. Rominger, M. Rudolph, A. S. K. Hashmi, *Chem. Commun.* **2016**, *52*, 6435–6438.

[26] S. Witzel, J. Xie, M. Rudolph, A. S. K. Hashmi, *Adv. Synth. Catal.* **2017**, *359*, 1522–1528.

[27] S. Witzel, K. Sekine, M. Rudolph, A. S. K. Hashmi, *Chem. Commun.* **2018**, *54*, 13802–13804.

[28] S. Taschinski, R. Döpp, M. Ackermann, F. Rominger, F. de Vries, M. F. S. J. Menger, M. Rudolph, A. S. K. Hashmi, J. E. M. N. Klein, *Angew. Chem., Int. Ed.* **2019**, *58*, 16988–16993.

[29] D. Eppel, M. Rudolph, F. Rominger, A. S. K. Hashmi, *ChemSusChem* **2020**, DOI: 10.1002/cssc.202000310.

[30] G. Albertin, S. Antoniutti, M. Bortoluzzi, J. Castro-Fojo, S. Garcia-Fontán, *Inorg. Chem.* **2004**, *43*, 4511–4522.

[31] X. Yan, F. W. B. Einstein, D. Sutton, *Can. J. Chem.* **1995**, *73*, 939–955.

[32] M. Daryanavard, D. Armstrong, A. J. Lough, U. Fekl, *Dalton Trans.* **2017**, *46*, 4004–4008.

[33] A. G. De Crisci, G. K. Hamer, U. Fekl, *J. Coord. Chem.* **2010**, *63*, 2928–2938.

[34] Á. Vivancos, D. Poveda, A. Muñoz, J. Moreno, D. Bautista, P. González-Herrero, *Dalton Trans.* **2019**, *48*, 14367–14382.

[35] F. Juliá, D. Bautista, P. González-Herrero, *Chem. Commun.* **2016**, *52*, 1657–1660.

[36] F. Juliá, M. D. García-Legaz, D. Bautista, P. González-Herrero, *Inorg. Chem.* **2016**, *55*, 7647–7660.

[37] M. Kasha, *Discuss. Faraday Soc.* **1950**, *9*, 14–19.

[38] N. Giménez, R. Lara, M. T. Moreno, E. Lalinde, *Chem. Eur. J.* **2017**, *23*, 5758–5771.

[39] N. Giménez, E. Lalinde, R. Lara, M. T. Moreno, *Chem. Eur. J.* **2019**, *25*, 5514–5526.

[40] J. S. Wilson, N. Chawdhury, M. R. A. Al-Mandhary, M. Younus, M. S. Khan, P. R. Raithby, A. Kohler, R. H. Friend, *J. Am. Chem. Soc.* **2001**, *123*, 9412–9417.

[41] H. S. Duan, P. T. Chou, C. C. Hsu, J. Y. Hung, Y. Chi, *Inorg. Chem.* **2009**, *48*, 6501–6508.

[42] Y. J. Cho, S. Y. Kim, M. Cho, K. R. Wee, H. J. Son, W. S. Han, D. W. Cho, S. O. Kang, *Phys. Chem. Chem. Phys.* **2016**, *18*, 15162–15169.
[43] S. Kumar, Y. Hisamatsu, Y. Tamaki, O. Ishitani, S. Aoki, *Inorg. Chem.* **2016**, *55*, 3829–3843.
[44] S. Ladouceur, L. Donato, M. Romain, B. P. Mudraboyina, M. B. Johansen, J. A. Wisner, E. Zysman-Colman, *Dalton Trans.* **2013**, *42*, 8838–8847.
[45] C. M. Cardona, W. Li, A. E. Kaifer, D. Stockdale, G. C. Bazan, *Adv. Mater.* **2011**, *23*, 2367–2371.
[46] M. Svobodová, P. Šimnek, V. MacHáček, L. Štruncová, A. Ržička, *Tetrahedron* **2012**, *68*, 2052–2060.
[47] G. M. Sheldrick, *Acta Crystallogr. Sect. A Found. Adv.* **2015**, *71*, 3–8.
[48] G. M. Sheldrick, *Acta Crystallogr., Sect. A Found. Crystallogr.* **2008**, *64*, 112–122.
[49] A. L. Spek, *Acta Crystallogr. Sect. C Struct. Chem.* **2015**, *71*, 9–18.
[50] Gaussian 09, Revision A.02, M. J. Frisch, G. W. Trucks, H. B. Schlegel, G. E. Scuseria, M. A. Robb, J. R. Cheeseman, G. Scalmani, V. Barone, B. Mennucci, G. A. Petersson, H. Nakatsuji, M. Caricato, X. Li, H. P. Hratchian, A. F. Izmaylov, J. Bloino, G. Zheng, J. L. Sonnenberg, M. Hada, M. Ehara, K. Toyota, R. Fukuda, J. Hasegawa, M. Ishida, T. Nakajima, Y. Honda, O. Kitao, H. Nakai, T. Vreven, J. A. Montgomery, Jr., J. E. Peralta, F. Ogliaro, M. Bearpark, J. J. Heyd, E. Brothers, K. N. Kudin, V. N. Staroverov, R. Kobayashi, J. Normand, K. Raghavachari, A. Rendell, J. C. Burant, S. S. Iyengar, J. Tomasi, M. Cossi, N. Rega, N. J. Millam, M. Klene, J. E. Knox, J. B. Cross, V. Bakken, C. Adamo, J. Jaramillo, R. Gomperts, R. E. Stratmann, O. Yazyev, A. J. Austin, R. Cammi, C. Pomelli, J. W. Ochterski, R. L. Martin, K. Morokuma, V. G. Zakrzewski, G. A. Voth, P. Salvador, J. J. Dannenberg, S. Dapprich, A. D. Daniels, Ö. Farkas, J. B. Foresman, J. V. Ortiz, J. Cioslowski, D. J. Fox, Gaussian Inc., Wallingford CT, 2009.
[51] A. Becke, *J. Chem. Phys.* **1993**, *98*, 5648–5652.
[52] C. T. Lee, W. T. Yang, R. G. Parr, *Phys. Rev. B* **1988**, *37*, 785–789.
[53] P. C. Hariharan, J. A. Pople, *Theor. Chim. Acta* **1973**, *28*, 213–222.
[54] M. M. Francl, W. J. Pietro, W. J. Hehre, J. S. Binkley, M. S. Gordon, D. J. Defrees, J. A. Pople, *J. Chem. Phys.* **1982**, *77*, 3654–3665.
[55] P. J. Hay, W. R. Wadt, *J. Chem. Phys.* **1985**, *82*, 299–310.
[56] D. Escudero, W. Thiel, *Inorg. Chem.* **2014**, *53*, 11015–11019.
[57] J. Tomasi, B. Mennucci, R. Cammi, *Chem. Rev.* **2005**, *105*, 2999–3093.
[58] E. D. Glendening, J. K. Badenhoop, A. E. Reed, J. E. Carpenter, J. A. Bohmann, C. M. Morales, F. Weinhold, **2009**.

Entry for the Table of Contents

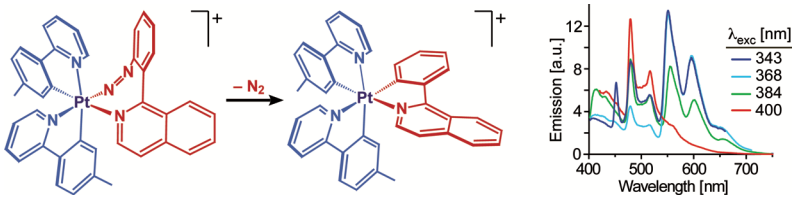

A stereoselective synthetic route to homo- and heteroleptic facial tris-cyclometalated Pt(IV) complexes is reported, which proceeds via chelating diazenide intermediates and allows the introduction of 2-arylpyridines of variable π-π^* transition energies. Dual phosphorescence from heteroleptic derivatives in rigid media is demonstrated.

Institute and/or researcher Twitter usernames: @pgherrero, @GqoLab